Performance Investigation of a Humpback Whale-Inspired Vertical Axis Current Turbine

Rizki Mendung Ariefianto[1,*] Rini Nur Hasanah[1,] Wijono[1,] Rizky Ajie Aprilianto[2]

[1] *Department of Electrical Engineering, Universitas Brawijaya, Malang, Indonesia*
[2] *Department of Electrical and Information Engineering, Universitas Gadjah Mada, Yogyakarta, Indonesia*
[*]*Corresponding author. Email: rizkimsahab19@gmail.com*

ABSTRACT
Efficiency and self-starting capability performances are the main problems in vertical axis current turbines (VACT). By purposing improves its performance, VACT has been developed with various models. One development of this model is designing the turbine blade into a bio-inspired shape. The fluke and flipper of a humpback whale become an inspiration to design the VACT blade. This study aims to investigate the ability of a humpback whale-inspired turbine (HWIT) in terms of efficiency, symbolized by power coefficient (C_P), and self-starting capability, symbolized by static torque coefficient (C_{Ts}). HWIT turbine was designed by applying an extremities chord ratio (Λ), determined from the ratio between the upper and lower part of the humpback whale fluke. Moreover, NACA $63_4$021 foil, inspired by a humpback whale flipper, was used to create the main blade form of an HWIT. NACA 0018, another foil profile used as the main foil from the previous study, was applied as a comparator to NACA $63_4$021 foil. The simulation results using the QBlade software show that NACA $63_4$021 has an excellent agreement validation with the previous study, both numerically and experimentally. The results present that the optimal blade shape of HWIT is reached at $\Lambda = 0.5$. Also, HWIT using NACA $63_4$021 has higher efficiency of 0.335 and reaches self-starting capability at $\lambda_{min} = 2.2$ compared to HWIT using NACA 0018.

Keywords: *HWIT, NACA $63_4$021 foil, Darrieus turbine, efficiency, self-starting.*

1. INTRODUCTION

Renewable energy contribution as electrical energy sources has been increasing rapidly in recent years. It is taken as an effort to reduce fossil energy consumption, which has bad impacts such as environmental pollution and the greenhouse effect [1]. By 2050, renewable energy sources will increase to 85%, of which marine energy-based sources such as ocean waves, tidal, ocean currents, ocean thermals, and salinity will be involved [2].

Regarding the technology development for utilizing marine energy sources, energy sources originating from tidal currents and ocean currents have more promising prospects. It is because the energy source using turbine technology has been developed for years, so it is viewed as becoming a mature technology. Also, this condition is supported by the results of the Technology Readiness Level (TRL), in which wind turbine technology has a high grade to reach the stage of extensive deployment [3].

One of the turbines used for energy conversion systems such as tidal currents or ocean currents is a vertical axis turbine (VAT) type. This turbine has various advantages: an uncomplicated design and an easy manufacturing process with low production costs [4]. From a technical point of view, VAT can convert fluid velocity from all directions without a yawing mechanism [5], can work properly in environments with high turbulence [6], and electrical components such as generators can be placed on the surface [7]. From the environmental point of view, the application of VAT is more friendly to fish migration because it is more easily identified by the fish's view, thereby reducing the risk of injury to fish due to being swept away by turbines [8]. In addition, VAT is also expected to produce low wakes, which have a small risk of sedimentation processes and changes in the pattern of ocean currents in the vicinity. However, Hosseini and Goudarzi [9] stated, VAT has significant drawbacks especially in its low-efficiency performance and low self-starting capability [10].

A. D. Saputro et al. (Eds.): ICOSEAT 2022, ABSR 26, pp. 749–758, 2023.
https://doi.org/10.2991/978-94-6463-086-2_99

Furthermore, various methods have been conducted to obtain VAT better performance, such as modifying the foil, the rotor's shape, and the blades' shape [11]. The V-shaped blade turbine is one of the VAT turbines designed by modifying the blade shape of the Darrieus turbine into a “V” shape. In principle, this turbine has a blade shape similar to the fluke (tail) of a humpback whale. This turbine shape was also patented by Achard and Maitre [12], called the Achard-Maitre turbine. In subsequent developments, the V-shaped turbine is also called Trapezoidal-blade turbine [13], Delta-shaped turbine [14], or Arrow-shaped blade [15].

Modifying the Darrieus turbine into a V-shaped turbine produces a good self-starting capability with an efficiency of 0.32 conducted by Zanette et al. [13]. Also, in Mosbahi et al. [14] showed that the V-shaped blade turbine produces self-starting capability and good efficiency at the optimal blade sweep angle. The relatively high efficiency of the V-shaped blade turbine can be achieved by Su et al. [16], which produced a power coefficient of 0.375. This study also recommends the variation of leading-edge distance from its normal position based on the value of chord length.

Moreover, turbine performance can be influenced by the foil shape. It is very influential, mainly in producing the turbine's lift and drag coefficients. Several studies on foil have been carried out. In Mohammed [17] was investigated symmetrical and asymmetrical foils from various types of foils, such as NACA 63XXX, NACA 00XX, type A, type FX, and type S. As a result, symmetrical foils produce the highest efficiency in each type compared to asymmetrical foils. The symmetrical foil also has advantages such as being able to operate at a wider speed ratio, overcoming the delay in the stall phenomenon, overcoming the decrease in efficiency due to changes in fluid speed [17], and reducing the occurrence of negative torque during the initial rotation of the turbine [18].

The symmetrical foil often applied in research on turbines is the NACA 00XX type foil, which can improve turbine performance. Bio-inspired foils have been developed, including the NACA 63_4021 foil. This foil was developed from the inspiration for the cross-section of the humpback whale flipper. The excellent ability to swim with the condition of having an enormous mass is the main inspiration for designing the foil from the humpback whale flipper [19]. In several studies, the performance of the Darrieus turbine using the NACA 63_4021 foil has been successfully carried out using numerical and experimental methods. In Rawlings [20] a three-blade Darrieus turbine using NACA 63_4021 foil was tested. It produces the highest efficiency of 0.305. The results of these studies are the following used as validators in numerical-based studies such as those conducted by Marsh et al. [21] and Yasim et al. [22], which achieve the highest turbine efficiency of 0.285 and 0.322, respectively. Since the turbine used is a conventional Darrieus turbine with straight blades, self-starting capability can be a problem.

Therefore, the use of a V-shaped blade turbine combined with the NACA 63_4021 foil is proposed in this study, considering that the physiology of the humpback whale equally inspires both the blade shape and foil design. In this research, the proposed turbine called by humpback whale-inspired turbine (HWIT). In addition, it is essential to consider the solidity factor in designing a VAT turbine. This factor is influenced by the turbine radius, the length of the foil chord, and the number of blades. The open-source QBlade software was used to simulate the proposed turbine idea. This software can be relied on in many studies because it has a double multiple streamtube (DMST) theoretical basis to simulate and improve turbines performance [23]. In many studies, this software also provides a good design and validation description to achieve an overview of the turbine performance [24].

2. METHOD

2.1 DMST-Based VAT Numerical Modeling

The high interest in VAT turbine research has encouraged the development of a numerical approach, one of which is realized through the QBlade software. The wind energy group initiated this software at the Technical University of Berlin, led by Prof. Christian Oliver Pascherit. This project aims to provide open-source turbine calculation software integrated into XFOIL, design tools, and foil analysis.

QBlade is designed based on the blade element momentum (BEM) model, which combines the blade element theory with momentum theory and is introduced to investigate the flow and force behavior of the turbine blades [25]. BEM theory has much less computational time than CFD [26], so the simulation is relatively fast [27]. In addition, the level of ease and high accuracy makes the BEM theory tend to be favoured [28]. Recent researchs have exhibited good agreement between the BEM theoretical code and the experimental turbine results [29].

Based on the BEM theory, several models have been developed, starting with the development of the single-stream tube (SST) model, which Templin first introduced in 1974. In this model, the turbine is placed in a unique flow tube surrounding the entire turbine. The subsequent development is a multiple stream tube (MST) model developed by Strickland in 1975. This model consists of several parallel flow tubes adjacent to each other. A more comprehensive approach, including field testing and software development, leads to the model introduced by Paraschivoiu, the double-multiple stream tube (DMST) model. This model considers the fluid flowing in the

circular path of the blades, so the energy extraction can be carried out in the upstream and downstream sections in the two actuator disc models [30], as illustrated in Figure 1.

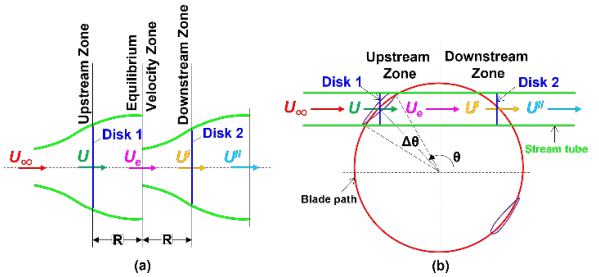

Figure 1 (a) Schematic of two actuator disc (b) DMST model

DMST model tries to overcome the weakness of the MST model in distinguishing between the upstream and downstream parts of the turbine. Hence, the two actuator discs are divided into two regions representing the upstream ($-\pi/2 \le \theta \le \pi/2$) and downstream ($\pi/2 \le \theta \le 3\pi/2$) of the rotor. The induced velocity for each flow tube upstream and downstream is represented by V_u and V_d, respectively, which both velocities have an interference factor concerning free stream velocity (V_∞) and equilibrium velocity (V_e) [31] as the following equation:

$$V_u = a_u V_\infty \tag{1}$$

$$V_e = (2a_u - 1)V_\infty \tag{2}$$

$$V_d = a_d V_e = a_d(2a_u - 1)V_\infty \tag{3}$$

where a_u and a_d are interference factors in the upstream and downstream areas, respectively, with $a_d < a_u$.

Furthermore, the local relative velocity (W) and angle of attack (α) for the upstream half cycle are given by:

$$W = V_\infty \sqrt{1 + 2\lambda\cos\theta + \lambda^2} \tag{4}$$

$$\alpha = \tan^{-1}\left(\frac{\sin\theta}{\cos\theta + \lambda}\right) \tag{5}$$

where θ is the blade azimuth angle and λ is the tip speed ratio (TSR) with the formula as follows:

$$\lambda = \frac{R\omega}{V_\infty} \tag{6}$$

for R is the turbine radius (m) and ω is the turbine angular speed (rad/s).

When the existing velocity is applied to a foil, there will be a lift force (L) and a drag force (D) with the coefficients given by:

$$C_L = \frac{L}{\frac{1}{2}\rho V_\infty^2 A} \tag{7}$$

$$C_D = \frac{D}{\frac{1}{2}\rho V_\infty^2 A} \tag{8}$$

with C_L is the lift coefficient, C_D is the drag coefficient, ρ is fluid density (kg/m^3), A is the rotor sweep area (m^2).

By involving C_L and C_D into the equations for the tangential force (F_t) and the normal force (F_n), the equation is obtained as follows:

$$F_t = \tfrac{1}{2}\rho HNcW^2\left[C_L\cos\alpha + C_D\sin\alpha\right] \tag{9}$$

$$F_n = \tfrac{1}{2}\rho HNcW^2\left[C_L\sin\alpha - C_D\cos\alpha\right] \tag{10}$$

H is the variable of the turbine height (m), and N is the number of blades. Furthermore, to obtain the average tangential force (F_{ta}) around the rotor and the azimuth angle, the formula is expressed by:

$$F_{ta} = \frac{1}{2\pi}\int_0^{2\pi} F_t(\theta)d\theta \tag{11}$$

so, the total torque (Q_t) and total power (P_t) can be calculated by:

$$Q_t = F_{ta}R \tag{12}$$

$$P_t = Q_t\omega \tag{13}$$

In the end the average power coefficient (C_P) and torque coefficient (C_T) can be obtained as follows:

$$C_P = \frac{P_t}{\frac{1}{2}\rho A V_\infty^2} \tag{14}$$

$$C_T = \frac{Q_t}{\frac{1}{2}\rho A V_\infty^2 R} \tag{15}$$

Another parameter determining VAT performance is solidity, which is defined by:

$$\sigma = \frac{Nc}{R} \tag{16}$$

for c is the length of the blade chord (m).

2.2. Simulation Steps

The simulation was carried out using QBlade software with the following steps: (1) Insert and analyze foil profiles with XFOIL direct analysis; (2) Extrapolate C_L and C_D on AoA 360° using the Montgomerrie-Viterna method; (3) Design and optimize turbine blades; (4) Simulate the turbine rotor with DMS Simulation; and (5) Simulate turbine power result.

The NACA 63$_4$021 foil was inspired by humpback whale flipper, as shown in (Figure 2a) referring to a study by [32]. In the initial stage, this foil is simulated by entering the coordinates with the extension .dat to obtain a foil image, as shown in Figure 2b. After it is formed, the number of coordinates can be increased or decreased to be exported into a new foil coordinate. To get the improvement, another foil was also tested, namely the NACA 0018 foil, which is the reference V-shaped blade turbine foil used in [13]. The lift coefficient and drag coefficient ratio (C_L/C_D) analysis is performed using

XFOIL direct analysis. This feature is used massively in foil study software because it can estimate foil performance with accurate results [33]. The foil is simulated at the angle of attack interval between 0° to 30° at the Reynolds number (*Re*) of 275000, which was also implemented in [13].

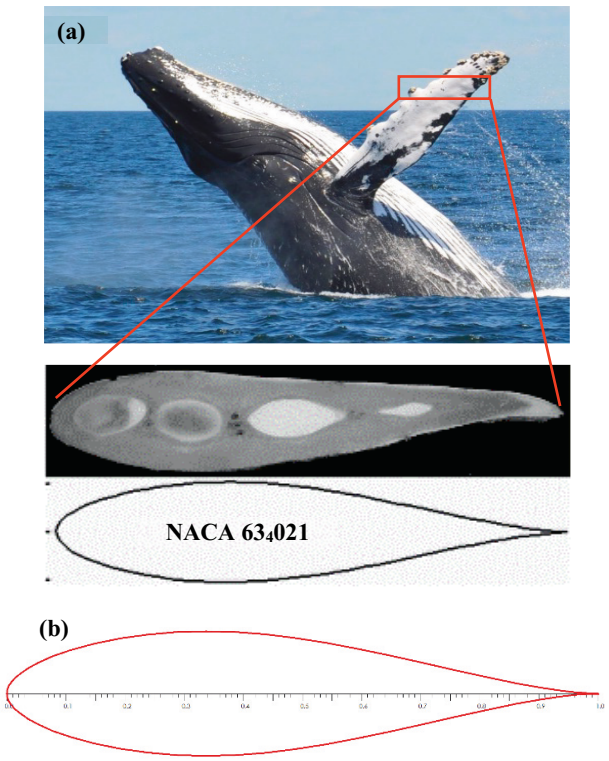

Figure 2 NACA 63$_4$021 foil profile (a) humpback whale flipper inspired, and (b) foil implementation

The geometric properties reference of HWIT originated from Zanette et al. [13], which is presented in Table 1. HWIT uses three blades because it gives good performance to a turbine in many studies. Also, HWIT has an aspect ratio of about two from the ratio value between turbine height to turbine radius. A blade swept angle of about 30° is chosen because it gives optimal self-starting capability [14]. This blade swept angle is also used [13]. The extremities chord ratio (Λ) is varied by keeping the mean chord length constant. This scheme aims to obtain the best humpback whale fluke form, as shown in Figure 3. In Table 2, it is essential to set Λ with minimum and the maximum ratio between 0.2 – 0.5, so the fluke can be close to its actual form.

Each turbine blade is divided into eight equal segments based on the blade height. This division aims to ease the illustration of the turbine in the QBlade software. Moreover, this segmentation is usually applied to analyze the use of different types of foil in one turbine blade. HWIT is designed by conditioning the "V" shape direction according to the direction of the leading edge. It is conducted because the fluid flow will pass through the leading edge to the trailing edge. Practically, each turbine blade will be connected by a profiled arm to the shaft to become a complete turbine unit. The three-dimensional design of the HWIT with the segmentation created in the QBlade software is shown in Figure 4.

Table 1. Geometric properties of HWIT

Variable	Value
Number of blades (N)	3
Turbine height (H)	0.5 m
Turbine radius (R)	0.25 m
Mean chord length (c_m)	0.09 m
Blade sweep angle (γ)	30°
Solidity (σ)	1.1
Reynolds number (Re)	275000
Tidal/ocean current speed (U_∞)	3 m/s

Table 2. The variation of extremities chord ratio

Λ	c_m (m)	c_u (m)	c_l (m)
0.2	0.09	0.03	0.15
0.3	0.09	0.04	0.14
0.4	0.09	0.05	0.13
0.5	0.09	0.06	0.12

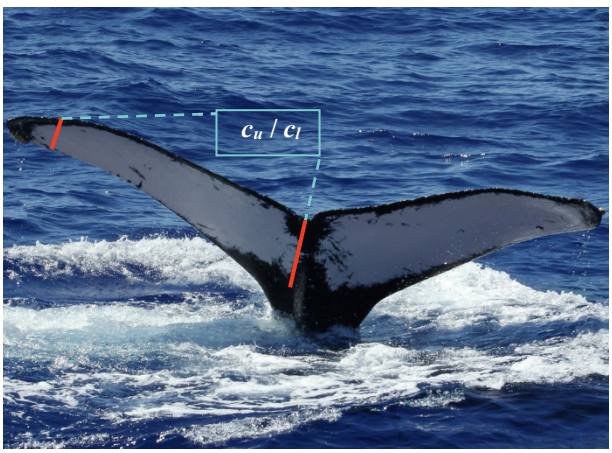

Figure 3 Humpback whale fluke ratio determination

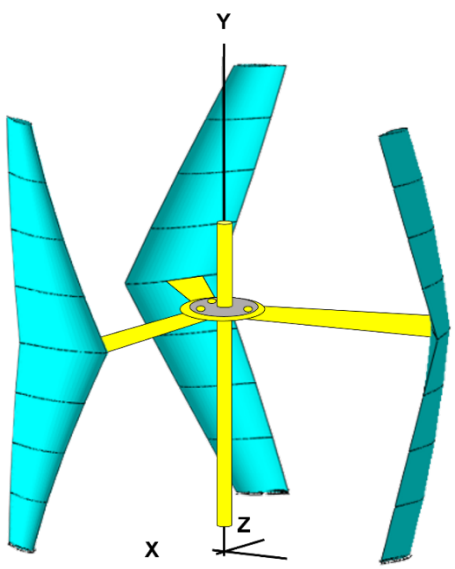

Figure 4 The HWIT design

3. RESULTS AND DISCUSSION

3.1. NACA 63$_4$021 Foil Validation Results

The NACA 63$_4$021 foil, designed to be a V-shaped blade turbine, is validated by previous research. The first validation was carried out regarding research from [34] at the same Reynolds number of 180,000. As shown in Figure 5, the validation results show that both the lift coefficient and the drag coefficient have followed the curve track-line very well, especially in pre-stall conditions. On the lift coefficient curve, there is a linear increase from AoA 0° to 12°, with good agreement with reference. A slightly slower increase occurs from AoA 12° to 18° until it stalls around AoA 20°. After passing the stall, the lift coefficient also seems to still have a suitable track-line up to AoA 30°.

Furthermore, a linear increase with the same characteristics is also experienced by the drag coefficient. This increase started from AoA 0° to 18° and then experienced a significant increase as the lift coefficient decreased in the stall condition. However, the characteristics become slightly different after this phase, especially after passing AoA 18°. The QBlade simulation results have a lower drag coefficient value than the results of other experimental and numerical studies in the post-stall area. The difference to this experiment result is indeed quite far, but it is still in the same increasing movement.

The validation of the NACA 63$_4$021 foil was also carried out on another Reynolds number of 183,000, with the result is shown in Figure 5. Initially, all studies produced the lift and the drag coefficients at almost the same value. However, in the present study, it appears to stall earlier when it reaches AoA 18°. In more detail, the same stall position is also possible in [35]. Meanwhile, the results from [32] and [36] only occur when the stall reaches AoA 20°. This condition indicates that the numerical result is appropriate enough compared to the experimental results.

From the validation results on the two different Reynolds numbers, it can be concluded that the lift coefficient review has shown results that follow previous studies. However, there is a slight discrepancy in the post-stall conditions. While in terms of drag coefficients, the pre-stall results on the Reynolds number 180,000 have a better trend than the Reynolds number 183,000. However, in post-stall conditions, the more suitable drag coefficient occurs at the Reynolds number of 183,000. Referring to the differences that occur, especially in the studies of [36] and [35] the characteristics of the resulting coefficients are still acceptable even though there are slight differences in the experimental results. In general, simulations using QBlade produce good validation of the experiment, as described in [29].

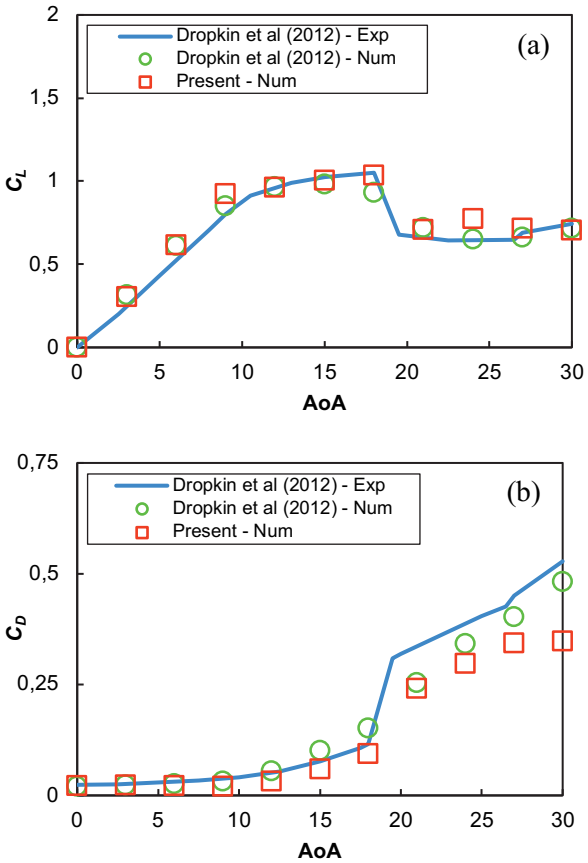

Figure 5 Characteristic validation of NACA 63$_4$021 foil with Re = 180,000 (a) AoA vs C_L, (b) AoA vs C_D

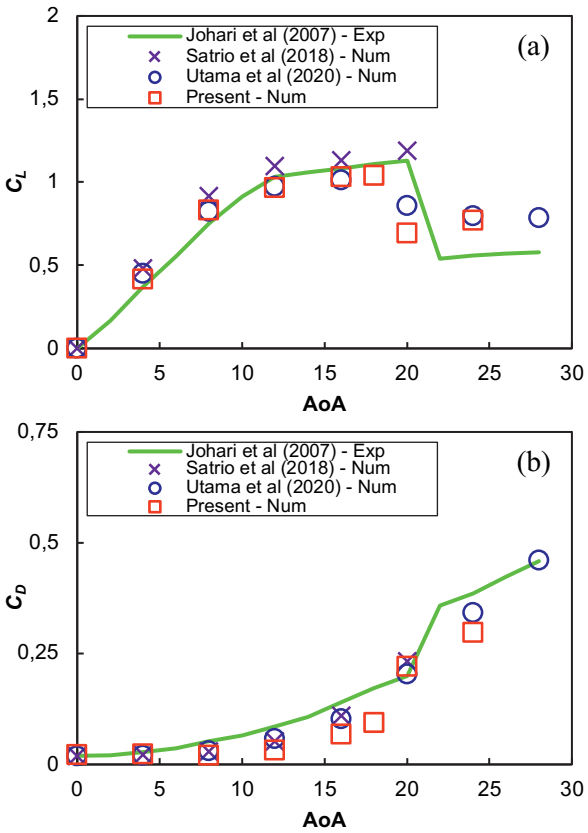

Figure 6 Characteristic validation of NACA 63$_4$021 foil with Re = 183,000 (a) AoA vs C_L, (b) AoA vs C_D

3.2. Effect of Extremities Chord Ratio

Extremities chord ratio is used to describe the shape of the humpback whales fluke by comparing the fluke tip and the "V" shape of the fluke, which is called notch. The configuration of Λ is determined by the best power curve generated. Based on the tested Λ configuration, the results are shown in Figure 7. In general, the resulting power coefficients are close to each other, but at a higher power coefficient and a wider-ranging tip speed ratio can be achieved. It is obvious that the larger Λ, the higher the power coefficient is obtained. Therefore, Λ = 0.5 can be considered for HWIT geometric aspect in the next step.

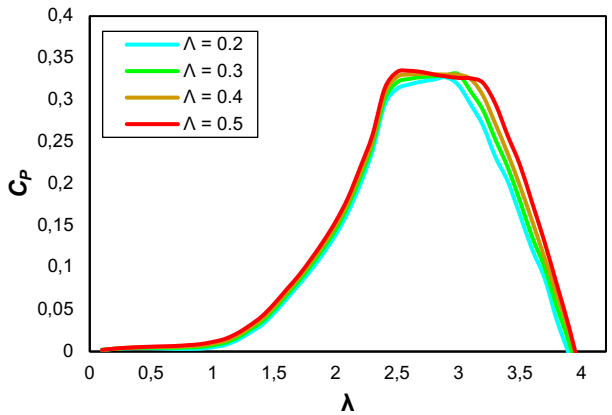

Figure 7 Power curve characteristic of extremities chord ratio effect

3.3 Efficiency Performance

After getting the appropriate extremities chord ratio, the next step is to analyze the results of the proposed turbine. HWIT designed using NACA 63$_4$021 foil was compared to HWIT using NACA 0018 foil, with the results shown in Figure 8a. These results indicate that NACA 63$_4$021 can produce a maximum C_P of 0.335, higher than the maximum C_P of the NACA 0018 foil of 0.329 at the same λ = 2.6. Using the same geometric properties of the turbine, the simulation results are also close to the performance of the Trapezoidal-shaped turbine, which produces a maximum C_P of 0.32 at λ = 2.5 [13]. It is also seen that at the initial λ, the HWIT turbine with NACA 63$_4$021 foil consistently has higher C_P than the HWIT turbine with NACA 0018 foil until λ = 3.3. This advantage cannot be separated from the lift coefficient to drag coefficient ratio (C_L/C_D) of NACA 63$_4$021 foil which is quite large compared to NACA 0018 foil, as shown in Figure 8b. For the similar position of angle of attack (α) at 9°, the NACA 63$_4$021 foil produces a C_L/C_D of 62.4 while the NACA 0018 foil produces a C_L/C_D of 48.7. However, using NACA 63$_4$021 foil has a range of $0 < \lambda < 3.9$, which is narrower than NACA 0018 foil with a range of $0 < \lambda < 4.2$.

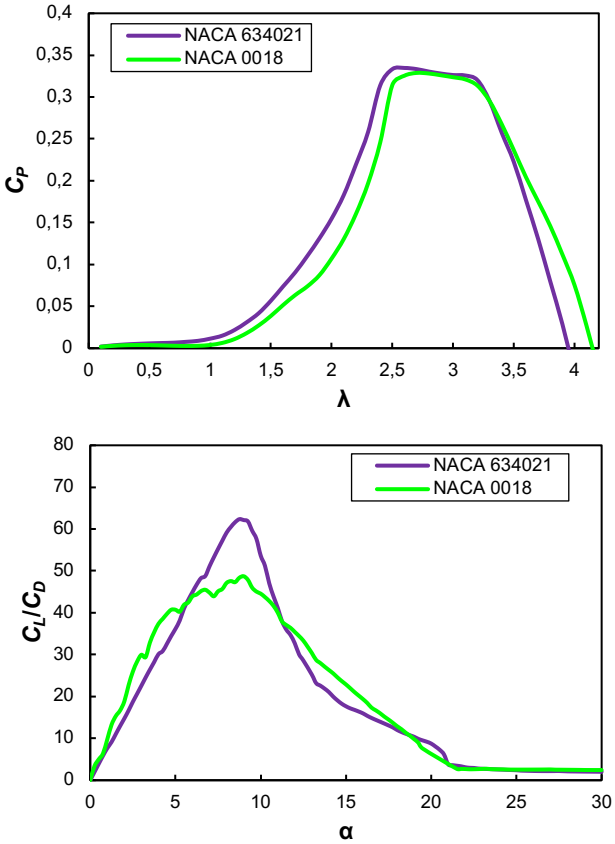

Figure 8 Comparison between NACA 63$_4$021 and NACA 0018 (a) C_P, and (b) C_L/C_D

3.4. Self-Starting Capability

Furthermore, to compare the self-starting capability of the turbine, it can be analyzed at a value of λ = 2, considering that the Darrieus type turbine must have a tip speed of at least twice the speed of the flowing fluid [37]. Another characteristic is that the Darrieus turbine has a negative torque, so it cannot rotate in the range $0 < \lambda < 2$ [38]. Self-starting capability is usually represented by static torque coefficients (C_{Ts}), with the comparison results shown in Figure 9. It can be analyzed that the use of NACA 63$_4$021 foil can provide good self-starting capability on the HWIT because it produces positive C_{Ts} along the azimuth angle at a minimum tip speed ratio λ_{min} = 2.2. At the same λ, the HWIT using NACA 0018 foil cannot rotate.

This result means that the NACA 63$_4$021 foil can help the turbine produce a minimum torque to rotate or can help generate enough power to compensate the mechanical friction in the turbine. After getting the initial rotation, the turbine can accelerate until it reaches its operating angular speed. Referring to the results and analysis of the application of the NACA 63$_4$021 foil on a HWIT, it can be summarized that the efficiency and self-starting capability produced achieve better performance when compared to the NACA 0018 foil.

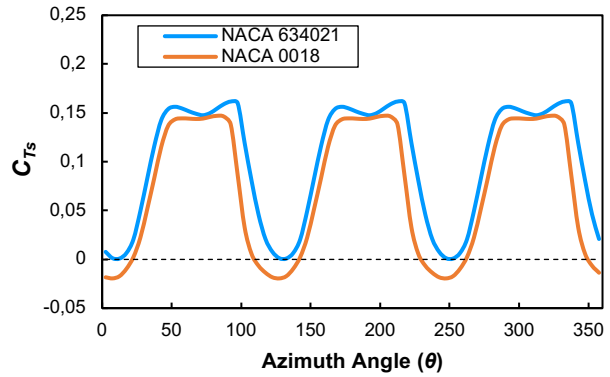

Figure 9 Static torque comparison between NACA 63$_4$021 and NACA 0018

3.5. Extracted Power

Furthermore, a DMS-based simulation was carried out to determine the power generated by the turbine. Maximum power is maintained at the optimum value of λ, which produces the highest efficiency. For the HWIT using NACA 63$_4$021 foil, optimum tip speed ratio is reached at $\lambda = 2.6$, which can use the pitch angle control method or maximum power point tracking (MPPT) to keep that value remain constant. The results of maximum power extraction for each change in ocean current speed are shown in Figure 10. It can be seen that the higher the ocean current speed extracted by the turbine, the greater the power converted. When the ocean current speed rating is around 3 m/s, a turbine power of around 1158 W can be obtained. The higher the turbine efficiency, the closer the available power can be extracted. Also, when the turbine reaches the current speed for its rating of 3 m/s, it is at the cut-off speed point so that at speeds greater than this value, the turbine power will be constant according to each rating. This effort is conducted to make turbine components more sustainable and reduce the damage risk. In the case of an ocean current power plant development, the required power will be determined earlier. Various options can be carried out to achieve this power needed, such as increasing the turbine sweep area by scaling dimensions or increasing the number of turbines used.

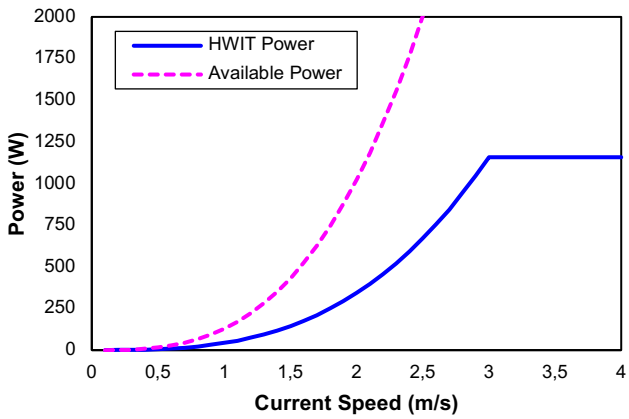

Figure 10. Extracted power of HWIT

4. CONCLUSION

In this study, HWIT, one of the Darrieus turbine types motivated by the physiology of the humpback whale, has been investigated using the QBlade software. Principally, the shape of the HWIT blade is inspired by a humpback whale fluke, which has a "V" shape, while the HWIT foil is inspired by the flipper shape of the same fish, so the NACA 63$_4$021 foil was chosen. As a result, the optimal blade configuration was achieved at the extremities chord ratio of 0.5. In addition, applying the NACA 63$_4$021 foil can make HWIT produce good performance with a CP achievement of 0.335 and has self-starting capability at $\lambda = 2.2$ compared to HWIT using NACA 0018 foil. Validation of the NACA 63$_4$021 foil also shows good agreement, both numerically and experimentally. Finally, as a preliminary study, the performance of HWIT can be known and considered for a more comprehensive extraction of ocean current energy potential.

ACKNOWLEDGMENTS

The authors would like to thank gratefully for the grants and the research funding from the Indonesia Endowment Fund for Education (LPDP), Ministry of Finance of The Republic of Indonesia for our master study.

REFERENCES

[1] R. M. Ariefianto, R. A. Aprilianto, H. Suryoatmojo, and S. Suwito, "Design and Implementation of Z-Source Inverter by Simple Boost Control Technique for Laboratory Scale Micro-Hydro Power Plant Application," J. Tek. Elektro 13(2) (2021) 62–70. doi: 10.15294/jte.v13i2.31884.

[2] M. Shadman, C. Silva, D. Faller, Z. Wu, L. P. d. F. Assad, L. Landau, C. Levi and S. F. Estefen., "Ocean renewable energy potential, technology, and deployments: A case study of Brazil," Energies 12(19) (2019). doi: 10.3390/en12193658.

[3] C. Mazur, S. Hall, J. Hardy, and M. Workman, "Technology is not a barrier: A survey of energy system technologies required for innovative electricity business models driving the low carbon energy revolution," Energies 12(428) (2019) 1–13. doi: 10.3390/en12030428.

[4] A. Ahmad, A. Loya, M. Ali, A. Iqbal, F. M. Baig, and A. M. Afzal, "Roadside Vertical Axis Wind Turbine (VAWT): An Effective Evolutionary Design for Australian Highway Commuters with Minimum Dynamic Stall," Engineering 12(9) (2020) 601–616. doi: 10.4236/eng.2020.129042.

[5] S. Y. Cho, S. K. Choi, J. G. Kim, and C. H. Cho, "An experimental study of the optimal design parameters of a wind power tower used to improve the performance of vertical axis wind turbines," Adv. Mech. Eng. 10(9) (2018 1–10. doi:

10.1177/1687814018799543.

[6] J. Krishnaraj, S. Ellappan, and M. A. Kumar, "Additive Manufacturing of a Gorlov Helical Type Vertical Axis Wind Turbine," Int. J. Eng. Adv. Technol. 9(2) (2019) 2639–2644. doi: 10.35940/ijeat.b4116.129219.

[7] D. Satrio, I. K. A. P. Utama, and Mukhtasor, "Vertical Axis Tidal Current Turbine: Advantages and Challenges Review," Proceeding Ocean. Mech. Aerosp. -Science Eng., vol. 3, no. July, pp. 64–71, 2016, [Online]. Available: http://isomase.org/OMAse/Vol.3-2016/Section-1/3-7.pdf.

[8] L. Hammar, L. Eggertsen, S. Andersson, J. Ehnberg, R. Arvidsson, M. Gullström, and S. Molander., "A probabilistic model for hydrokinetic turbine collision risks: Exploring impacts on fish," PLoS One 10(3) (2015) 1–25. doi: 10.1371/journal.pone.0117756.

[9] A. Hosseini and N. Goudarzi, "Design and CFD study of a hybrid vertical-axis wind turbine by employing a combined Bach-type and H-Darrieus rotor systems," Energy Convers. Manag., vol. 189 (2018) 49–59. doi: 10.1016/j.enconman.2019.03.068.

[10] K. H. Wong, W. T. Chong, N. L. Sukiman, S. C. Poh, Y. C. Shiah, and C. T. Wang, "Performance enhancements on vertical axis wind turbines using flow augmentation systems: A review," Renew. Sustain. Energy Rev., vol. 73, pp. 904–921, 2017, doi: 10.1016/j.rser.2017.01.160.

[11] D. Satrio, I. K. A. P. Utama, and Mukhtasor, "Numerical Investigation of Contra Rotating Vertical-Axis Tidal-Current Turbine," J. Mar. Sci. Appl. 17(2) (2018) 208–215. doi: 10.1007/s11804-018-0017-5.

[12] J.-L. Achard and T. Maitre, "Hydraulic Turbo-machine, Applicant: INPG (FR)," 2004.

[13] J. Zanette, D. Imbault, and A. Tourabi, "A design methodology for cross flow water turbines," Renew. Energy 35(5) (2010) 997–1009. doi: 10.1016/j.renene.2009.09.014.

[14] M. Mosbahi, A. Ayadi, Y. Chouaibi, Z. Driss, and T. Tucciarelli, "Experimental and numerical investigation of the leading edge sweep angle effect on the performance of a delta blades hydrokinetic turbine," Renew. Energy, vol. 162 (2020) 1087–1103. doi: 10.1016/j.renene.2020.08.105.

[15] R. M. Ariefianto, R. N. Hasanah, and W. Wijono, "Unjuk Kerja Performa Turbin Arus Laut Sumbu Vertikal Pada Berbagai Bentuk Sudu Unik," Rekayasa 15(1) (2022) 53–63. doi: 10.21107/rekayasa.v15i1.13572.

[16] J. Su, Y. Chen, Z. Han, D. Zhou, Y. Bao, and Y. Zhao, "Investigation of V-shaped blade for the performance improvement of vertical axis wind turbines," Appl. Energy, vol. 260 (2020) 114326. doi: 10.1016/j.apenergy.2019.114326.

[17] M. H. Mohamed, "Performance investigation of H-rotor Darrieus turbine with new airfoil shapes," Energy 47(1) (2012) 522–530. doi: 10.1016/j.energy.2012.08.044.

[18] W. Wardhana and E. N. Fridayana, "Aerodynamic Performance Analysis of Vertical Axis Wind Turbine (VAWT) Darrieus Type H-Rotor using Computational Fluid Dynamics (CFD) Approach," in Proceedings of the 3rd International Conference on Marine Technology, 2018, no. Senta 2018, pp. 5–11, doi: 10.5220/0008542700050011.

[19] C. Cai, Z. Zuo, S. Liu, and Y. Wu, "Numerical investigations of hydrodynamic performance of hydrofoils with leading-edge protuberances," Adv. Mech. Eng. 7(7) (2015) 1–11. doi: 10.1177/1687814015592088.

[20] G. W. Rawlings, "Parametric Characterization of an Experimental Vertical Axis Hydro Turbine," Thesis, University of British Columbia, Vancouver, Canada, 2008.

[21] P. Marsh, D. Ranmuthugala, I. Penesis, and G. Thomas, "The influence of turbulence model and two and three-dimensional domain selection on the simulated performance characteristics of vertical axis tidal turbines," Renew. Energy, vol. 105, (2017) 106–116. doi: 10.1016/j.renene.2016.11.063.

[22] A. Yasim, Mukhtasor, S. Rahmawati, Widodo, and Madi, "Numerical Modeling of Vertical Axis Hydro Turbine with Experimental Validation," in Proceedings of the 7th International Seminar on Ocean and Coastal Engineering, Environmental and Natural Disaster Management, 2021, no. ISOCEEN 2019, pp. 22–29, doi: 10.5220/0010046900220029.

[23] F. Mahmuddin, "Rotor Blade Performance Analysis with Blade Element Momentum Theory," Energy Procedia, vol. 105 (2017) 1123–1129. doi: 10.1016/j.egypro.2017.03.477.

[24] M. R. Islam, L. Bin Bashar, and N. S. Rafi, "Design and Simulation of A Small Wind Turbine Blade with Qblade and Validation with MATLAB," 2019 4th Int. Conf. Electr. Inf. Commun. Technol. EICT 2019 vol. 3 (2019) 20–22. doi: 10.1109/EICT48899.2019.9068762.

[25] M. Moghimi and H. Motawej, "Developed DMST model for performance analysis and parametric evaluation of Gorlov vertical axis wind turbines," Sustain. Energy Technol. Assessments, vol. 37 (2020). doi: 10.1016/j.seta.2019.100616.

[26] S. N. Akour, M. Al-Heymari, T. Ahmed, and K. A. Khalil, "Experimental and theoretical investigation of micro wind turbine for low wind speed regions," Renew. Energy, vol. 116 (2018) 215–223. doi: 10.1016/j.renene.2017.09.076.

[27] P. A. Kulkarni, W. Hu, A. S. Dhoble, and P. M. Padole, "Statistical wind prediction and fatigue analysis for horizontal-axis wind turbine composite material blade under dynamic loads," Adv. Mech. Eng. 9(9) (2017) 1–26. doi: 10.1177/1687814017724088.

[28] O. Yirtici, K. Cengiz, S. Ozgen, and I. H. Tuncer, "Aerodynamic validation studies on the performance analysis of iced wind turbine blades," Comput. Fluids, vol. 192 (2019) 1–9. doi: 10.1016/j.compfluid.2019.104271.

[29] J. P. Monteiro, M. R. Silvestre, H. Piggott, and J. C. André, "Wind tunnel testing of a horizontal axis wind turbine rotor and comparison with simulations from two Blade Element Momentum codes," J. Wind Eng. Ind. Aerodyn., vol. 123 (2013) 99–106. doi: 10.1016/j.jweia.2013.09.008.

[30] N. Batista, R. Melicio, and V. Mendes, "Darrieus-type vertical axis rotary-wings with a new design approach grounded in double-multiple streamtube performance prediction model," AIMS Energy 6(5) (2018) 673–694. doi: 10.3934/ENERGY.2018.5.673.

[31] I. Paraschivoiu, O. Trifu, and F. Saeed, "H-Darrieus wind turbine with blade pitch control," Int. J. Rotating Mach., vol. 2009 (2009). doi: 10.1155/2009/505343.

[32] H. Johari, C. Henoch, D. Custodio, and A. Levshin, "Effects of leading-edge protuberances on airfoil performance," AIAA J. 45(11) (2007) 2634–2642. doi: 10.2514/1.28497.

[33] D.-H. Zhang, L. Ding, B. Huang, X.-M. Chen, and J.-T. Liu, "Optimization Study on the Blade Profiles of A Horizontal Axis Tidal Turbine Based on BEM-CFD Model," China Ocean Eng. 33(4) (2019) 436–445. doi: 10.1007/s13344-019-0041-5.

[34] A. Dropkin, D. Custodio, C. W. Henoch, and H. Johari, "Computation of flowfield around an airfoil with leading-edge protuberances," J. Aircr. 49(5) (2012) 1345–1355. doi: 10.2514/1.C031675.

[35] I. K. A. P. Utama, D. Satrio, Mukhtasor, M. Atlar, W. Shi, R. Hantoro, and G. Thomas, "Numerical simulation of foil with leading-edge tubercle for vertical-axis tidal-current turbine," J. Mech. Eng. Sci. 14(3) (2020) 6982–6992. doi: 10.15282/jmes.14.3.2020.02.0547.

[36] D. Satrio, I. K. A. P. Utama, and Mukhtasor, "Performance Enhancement Effort for Vertical-Axis Tidal-Current Turbine in Low Water Velocity," *4th Asian Wave Tidal Energy Conf.*, pp. 1–5, 2018, [Online]. Available: https://tethys-engineering.pnnl.gov/publications/performance-enhancement-effort-vertical-axis-tidal-current-turbine-low-water-velocity.

[37] G. L. Johnson, *Wind Energy System*. Manhattan: Kansas State University, 2006.

[38] S. Victor and M. Paraschivoiu, "Performance of a Darrieus turbine on the roof of a building," Trans. Can. Soc. Mech. Eng. 42(4) (2018) 341–349. doi: 10.1139/tcsme-2017-0096.